PCCP

Accepted Manuscript

This article can be cited before page numbers have been issued, to do this please use: L. Zhou, Q. Yan, J. Yu, R. J. R. Jones, N. Becerra-Stasiewicz, S. K. Suram, A. Shinde, D. Guevarra, J. Neaton, K. Persson and J. Gregoire, *Phys. Chem. Chem. Phys.*, 2016, DOI: 10.1039/C6CP00473C.

View Article Online
DOI: 10.1039/C6CP00473C

Journal Name

COMMUNICATION

Stability and Self-passivation of Copper Vanadate Photoanodes under Chemical, Electrochemical, and Photoelectrochemical Operation†

Received 00th January 20xx,
Accepted 00th January 20xx

DOI: 10.1039/x0xx00000x

www.rsc.org/

Lan Zhou,[a] Qimin Yan,[bc] Jie Yu,[bde] Ryan J. R. Jones,[a] Natalie Becerra-Stasiewicz,[a] Santosh K. Suram,[a] Aniketa Shinde,[a] Dan Guevarra,[a] Jeffrey B. Neaton,[bcf] Kristin A. Persson,[*e] and John M. Gregoire[*a]

Deployment of solar fuels technology requires photoanodes with long term stability, which can be accomplished using light absorbers that self-passivate under operational conditions. Several copper vanadates have been recently reported as promising photoanode materials, and their stability and self-passivation is demonstrated through a combination of Pourbaix calculations and combinatorial experimentation.

The solar-driven synthesis of fuel, which is performed by coupling the oxygen evolution reaction (OER) with fuel-forming hydrogen evolution or carbon dioxide reduction reactions, is a promising strategy for generating renewable energy.[1] Chemical fuels offer high energy density and facile distribution, and photoelectrochemical (PEC) cells with tandem light absorbers and liquid-semiconductor junctions are being developed into efficient solar fuels generators.[2] Widespread deployment of PEC solar fuels technology is impeded by several technological challenges, most notably the development of a stable photoanode that enables efficient photoelectrocatalysis of the OER.[2-3]

The coupling of solar light absorption with electrocatalysts enables efficient fuel generation but also poses substantial challenges with respect to the electrochemical stability of active components, particularly in the acidic or alkaline media that yield the highest device efficiencies.[4] A corresponding challenge for solar fuels research is the discovery of OER photoelectrocatalysts that exhibit stable operation in as high of a concentration of base as possible. Traditionally, with the notable exception of α-Fe_2O_3, the stability of low-band gap (below 2.5 eV) metal oxides has proved problematic.[5] In particular, compound metal oxide semiconductors such as bismuth vanadate ($BiVO_4$) suffer from rapid corrosion via anodic dissolution of V species.[6] In the present work we demonstrate that V corrosion is mitigated in copper vanadates through self-passivation.

A primary strategy for protection of light absorbers in aqueous electrolytes is the application of an inert, protective coating, which often lowers efficiency due to increases in electrical resistance and recombination rates.[7] Recent progress in defect engineering of protective metal oxide coatings has yielded efficient charge transport,[8] but scaling and deployment of light absorbers that do not self-passivate is untenable as the entire device can be destroyed from a single-point failure in the protective layer. Metal oxides are among the most stable materials in the highly oxidizing OER conditions,[5a] and several metal oxide photoelectrocatalysts have been recently identified in the CuO-V_2O_5 system.[9] These copper vanadates exhibit impressive PEC stability under several conditions, most notably in an aqueous borate buffer electrolyte with pH near 9.2, where stable photocurrent was observed over a 30 min experiment under toggled ultraviolet irradiation at the OER equilibrium potential ($E_{H2O/O2}$ = 1.23 V vs RHE).[9b]

To explore a thermodynamic description of this observed (photo)electrochemical stability, we construct the Pourbaix diagram of Cu-V-H_2O systems based on energetic information stored in the Materials Project database.[10] The construction of the Pourbaix diagram is based on the work of Persson *et al*.[11] Figure 1 shows the calculated Pourbaix diagram for $Cu_{0.5}V_{0.5}$ with solution ion concentrations of both Cu and V set to be 10^{-4} mol kg^{-1}. While the Pourbaix diagram is quite complex with over 20 unique phase fields, none of the copper vanadate ternary phases are stable. Several V and Cu binary oxide species are stable under various electrochemical conditions, as shown with the colored regions of the Pourbaix diagram. CuO and VO_2 coexist in a small region in the center of the Pourbaix diagram where each of the primary phases of interest (γ-$Cu_3V_2O_8$, β-$Cu_2V_2O_7$, α-$Cu_2V_2O_7$, α-CuV_2O_6, and $Cu_{11}V_6O_{26}$) are near 0.1 eV $atom^{-1}$ above the hull, the lowest above-hull energy observed

[a] Joint Center for Artificial Photosynthesis, California Institute of Technology, Pasadena, CA 91125, USA. Email: gregoire@caltech.edu
[b] Molecular Foundry, Lawrence Berkeley National Laboratory, Berkeley, CA 94720, USA.
[c] Department of Physics, University of California, Berkeley, CA 94720, USA.
[d] Joint Center for Artificial Photosynthesis, Lawrence Berkeley National Laboratory, Berkeley, CA 94720, USA.
[e] Environmental Energy Technologies Division, Lawrence Berkeley National Laboratory, Berkeley, CA 94720, USA. Email: kapersson@lbl.gov
[f] Kavli Energy NanoSciences Institute, Berkeley, CA 94720, USA.

† Electronic Supplementary Information (ESI) available: Experimental and calculation details and summary tables. See DOI: 10.1039/x0xx00000x

for these phases. CuO is also stable in mild to alkaline conditions near $E_{H2O/O2}$, but V dissolves as HVO_4^{2-} , $HV_2O_7^{3-}$ or VO_4^- under these conditions. At the $E_{H2O/O2}$ potential and pH 9.2, the condition where stable photoelectrocatalysis has been reported, the above-hull energies for these copper vanadates are 0.41 – 0.58 eV atom^{-1}. The resulting thermodynamic prediction is that V will corrode from these materials, leaving behind either solid CuO or Cu_2O_3, the latter being the equilibrium Cu species at potentials just above $E_{H2O/O2}$.

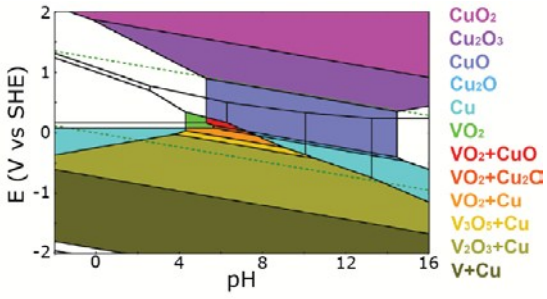

Figure 1 The calculated Pourbaix diagram for Cu-V-H_2O systems. The green dashed lines denote the water redox potentials. The regions with stable solid species are colored according to the key on the right.

Given the predicted instability of ternary copper vanadate photoelectrocatalysts, we turn to experimental measurements to further assess their stability under chemical, electrochemical and photoelectrochemical conditions. A suite of traditional techniques have been employed to investigate corrosion mechanisms,[12] and associated combinatorial implementations include characterization of oxidation resistance in air[13] and scanning electrochemical probes that monitor the concentration of dissolved species.[14] Given the variety of copper vanadate phases of interest, composition libraries offer a powerful ability to rapidly map stability with respect to composition and structure. Three $Cu_{1-x}V_xO_z$ thin film composition libraries (libraries A, B, and C) were synthesized by combinatorial sputtering and characterized using a combination of synchrotron and benchtop x-ray diffraction (XRD) techniques. Additional characterization with x-ray fluorescence (XRF) and energy-dispersive x-ray spectroscopy (EDS) measurements yielded composition-structure maps that provided the starting point for stability evaluation.

To assess stability under a variety of conditions the 3 libraries were tested as-follows: library A was soaked in electrolyte for 48 hours to assess chemical stability; library B was operated at $E_{H2O/O2}$ in a flow cell to assess electrochemical stability; library C was operated at $E_{H2O/O2}$ under AM 1.5 irradiation to assess photoelectrochemical stability. All experiments were performed in an aqueous electrolyte solution of 0.1 M boric acid with approximately 0.05 M potassium hydroxide, resulting in an electrolyte solution buffered at pH 9.2, per previous reports on OER photoelectrocatalysis.[9] After these experiments, the XRF or EDS composition measurements were repeated on the same library positions to quantify any corrosion-induced composition changes. To visualize how these compositions vary with the as-prepared composition and structure, the data are compiled into a series of graphics in Figure 2. The 3 sub-panels provide the results for libraries A, B, and C, respectively, where the abscissa of each plot corresponds to the composition of the as-prepared library. The phase map of each library is shown as a colored stack plot; at a given composition, a vertical cross-section of the stack plot provides the molar ratios of the various copper vanadate phases. A total of 8 different phases are observed in the libraries with variations in phase behavior resulting from different synthesis conditions, as detailed in the ESI.† It is worth noting that phase regions are labeled by the stoichiometry of the observed structure, and any alloying (site substitution) within these phases has not been characterized.

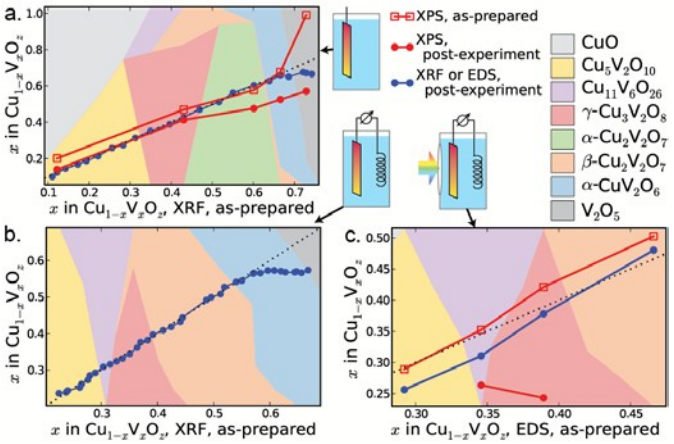

Figure 2. The composition, V/(V+Cu), of the bulk and near-surface before and after a (a) 48 hour chemical soak of library A, (b) 2 hour electrochemical operation of library B, and (c) 40 min PEC operation of library C. The phase fraction of each composition library obtained by XRD analysis is shown with a background color stack plot according to the 8-phase color legend shown in the upper-right. Illustrations of the 3 types of experiments are also shown along with the legend in the upper-right portion of the figure.

To visualize corrosion-induced composition changes, the compositions measured after each stability experiment are plotted on the ordinate axis, and the dotted black line corresponds to no composition change. Inspection of the XRF data for libraries A and B reveals that the majority of composition samples exhibit excellent compositional stability. In particular, the previously-reported OER photoelectrocatalysts, α-$Cu_2V_2O_7$, β-$Cu_2V_2O_7$, γ-$Cu_3V_2O_8$, and $Cu_{11}V_6O_{26}$,[9b] are all found to retain their as-prepared composition during the chemical and electrochemical experiments. In these experiments, composition changes are only observed with $x > 0.67$ for library A and $x > 0.57$ for library B. Comparing the composition changes to the underlying phase maps indicates that V loss coincides with the presence of V_2O_5 phase in the chemical soak and with both α-CuV_2O_6 and V_2O_5 in the electrochemical experiment.

Given the substantial electrochemical V corrosion for $x > 0.57$, the photoelectrochemical experiments (library C) were limited to phase-pure samples with $x < 0.5$. For the β-$Cu_2V_2O_7$ and γ-$Cu_3V_2O_8$ phases, the composition change resulting from the 40 min photoelectrochemical operation is within the uncertainty of the EDS

measurements. The V concentration loss for $Cu_{11}V_6O_{26}$ and $Cu_5V_2O_{10}$ samples is less than 0.05, which is larger than the V loss in the electrochemical experiment. For all 4 phases, the photoelectrochemical corrosion is limited compared to that expected from the Pourbaix thermodynamics.

Further insight is provided by x-ray photoelectron spectroscopy (XPS) measurements on libraries A and C (see ESI for experiment and analysis details). As shown in Fig. 2a, the as-prepared XPS composition is similar to the as-prepared XRF composition for each copper vanadate phase. After the 48 hour chemical soak, a small loss of V is observed in the XPS measurements of the Cu-rich samples, while the V-rich samples have XPS compositions that are approximately 0.13 lower than the respective bulk compositions. The V concentration loss is much more pronounced in the near-surface XPS measurement than in the bulk measurement. This phenomenon is even more apparent in the photoelectrochemical experiments on $Cu_{11}V_6O_{26}$ and γ-$Cu_3V_2O_8$ (library C), where the near-surface composition falls to approximately $x = 0.25$ for these Cu-rich samples despite relatively small changes in the bulk composition. These observations provide strong evidence of a self-passivation process in which V corrodes from the film, leaving behind a Cu-rich oxide surface layer that mitigates further V corrosion through a kinetic hindrance of both V migration to the surface and electrolyte penetration to the V.

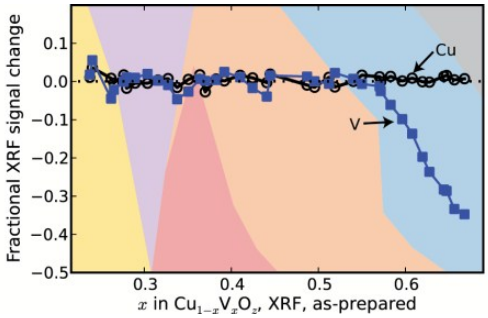

Figure 3. Fractional XRF signal change for both Cu and V after 2 hours of polarization at $E_{H2O/O2}$ (library B). The phase concentration map is the same as in Figure 2b.

As noted in the Pourbaix diagram of Figure 1, the stable CuO and Cu_2O_3 species enable self-passivation and suggest that Cu may not corrode from the copper vanadate phases. To assess electrochemical Cu corrosion, a complementary representation of the XRF characterization of library B is shown in Figure 3. Since the sampling depth of the XRF measurement is much larger than the film thickness, the elemental XRF intensity is approximately proportional to total amount of that element in the sample, enabling the corrosion of each element to be independently quantified. No loss of V or Cu is observed in this electrochemical experiment for $x < 0.57$ compositions. At V-rich compositions that exhibited V concentration loss (Figure 2b), the Cu signal remains unchanged and the extent of V corrosion increases with the as-prepared V concentration (Figure 3). This trend is commensurate with a self-passivation model in which the dynamic formation of a Cu oxide protective coating relies on V corrosion, and with an initially dilute Cu concentration in the near-surface, substantial V corrosion proceeds prior to passivation. The observation that the bulk V loss approaches 0 at $x = 0.57$ instead of $x = 0$ indicates that the protective coating on the Cu-rich phases is very thin under these electrochemical conditions.

The formation of a passivation layer may be deleterious to photoelectrochemical performance by impeding charge transport or introducing oxygen vacancy defects that increase recombination. In library C, the substantial V loss observed in the XPS measurements indicates that the passivation layer is relatively thick. In the ESI, we summarize the photocurrent stability of several copper vanadate phases using various illumination sources, including results from previous reports. Our photoelectrochemical measurement on Library C is the only measurement in which substantial degradation in photocurrent is observed within 30 minutes of operation, and it appears to be the only measurement in which intense infrared illumination on a thin electrochemical cell yields substantial temperature rise during the measurement. These results indicate that while the copper vanadate phases self-passivate against corrosion, the operational stability of these photoelectrocatalysts hinges upon keeping the passivation layer below a critical thickness, which may require limiting the operating temperature.

A more detailed analysis of the XPS measurements provides further understanding of the native protective coating. Figure 4 shows the survey spectra and high-resolution core level spectra of γ-$Cu_3V_2O_8$ before and after the 40 min PEC stability measurement, which are interpreted using a detailed XPS study of Cu and V oxides by Biesinger et al.[15] The Cu 2p and V 2p core level spectra of the as-prepared film are well matched to standard spectra for CuO and V_2O_5 with a small fraction of Cu^{1+}, suggesting that the surface of γ-$Cu_3V_2O_8$ phase can be reduced in ambient air or XPS high vacuum conditions. Formation of Cu^{1+} can also be mediated by surface oxygen vacancies[16] and, if formed, may contribute to increased corrosion as the very mobile Cu^{1+} ions are known to be less stable under high potential in aqueous conditions. Hence, exploring the change in surface speciation after photo-illumination is important.

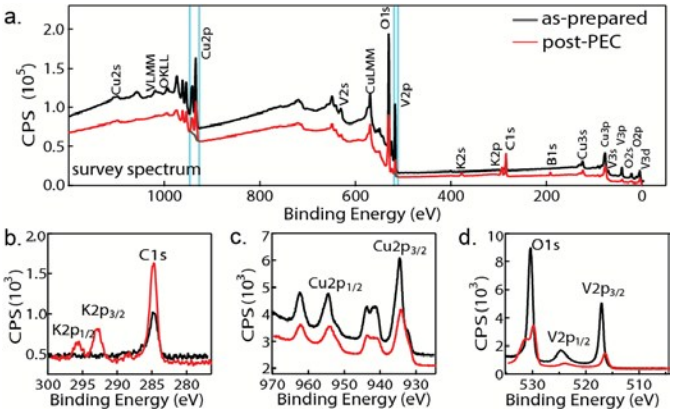

Figure 4. XPS spectra for the $x = 0.39$ composition sample (γ-$Cu_3V_2O_8$) from library C before and after 40 min PEC stability measurement in pH 9.2 at $E_{H2O/O2}$ under AM 1.5 illumination. (a) Survey spectra with highlighted Cu $2p_{3/2}$ and V $2p_{3/2}$ peak regions used for the quantification of Cu:V. The high-resolution core-level XPS spectra are also shown for (b) C 1s and K 2p, (c) Cu 2p, and (d) V 2p and O 1s.

After the photoelectrochemical operation, the library was removed under potential control with AM 1.5 illumination and a dry N_2 stream was used to remove electrolyte solution. As shown in Fig. 4c, Cu 2p spectra remain largely unchanged by the 40 min PEC operation with a slight shift of Cu $2p_{3/2}$ to lower binding energy. The V 2p spectra show a substantial decrease in signal intensity with the V 2p doublet peaks shifting to values closer to the published values for VO_2, which is stable over much of the Pourbaix diagram. The corrosion process on the surface under illumination likely creates oxygen vacancies, which are the most commonly observed defects on oxide surfaces[17] and would facilitate the appearance of V^{4+} in the XPS measurement.[18] While detailed analysis of the O 1s signal is hampered by adventitious hydrocarbons, the signal is clearly changed by the PEC experiment, which may be due to the formation of a metal hydroxide(s) during operation in the alkaline electrolyte. These observations confirm that during photoelectrochemical operation, the Cu is mostly retained and remains predominantly in a Cu^{2+}-like state. We surmise that the generation of any Cu^{1+} (dissolved or retained at the interface) is small.

The other notable feature in the post-photoelectrochemistry measurements is the appearance of signals from the electrolyte elements K and B. Despite the attempted removal of electrolyte from the library during extraction, the XPS characterization of γ-$Cu_3V_2O_8$ and $Cu_{11}V_6O_{26}$ (Figure 4) exhibit small K and B signals that may be from sparse islands of precipitated salts or a more conformal coating resulting from complexation with the transition metal oxide surface. The complexation of the borate electrolyte may facilitate the passivation process and is commensurate with the exceptional stability of copper vanadates in pH 9.2 borate buffer compared to pH 7 phosphate buffer and pH 13 sodium hydroxide.[9] Indeed, the Pourbaix thermodynamic calculations indicate that at $E_{H2O/O2}$, the energetic instability of the copper vanadates monotonically increases from pH 7 to pH 13, motivating future study of the role of the borate buffer in corrosion passivation.

Given the self-passivation model, the Cu-rich photoelectrocatalysts $Cu_{11}V_6O_{26}$ and γ-$Cu_3V_2O_8$ remain of greatest interest for further development of solar fuels photoanodes. While the extensive recent efforts in atomic layer deposition of protective coatings has yielded conformal coatings and high quality interfaces, protective coatings formed by self-passivation cannot be rivaled in conformality, compactness, and self-healing properties. Decade-long stability of photoelectrochemical materials will be most readily attained using self-passivating materials, prompting development of semiconductors whose native protective coatings remain functional. The copper vanadates have emerged as the most promising set of such photoanodes, particularly in weakly alkaline borate electrolytes.

Notes and references

This manuscript is based upon work performed by the Joint Center for Artificial Photosynthesis, a DOE Energy Innovation Hub, supported through the Office of Science of the U.S. Department of Energy (Award No. DE-SC0004993). Computational work was supported by the Materials Project (DOE Grant # EDCBEE) through the U.S. Department of Energy, Office of Basic Energy Sciences, Materials Sciences and Engineering Division, under Contract No. DE-AC02–05CH11231. Use of the Stanford Synchrotron Radiation Lightsource is supported by the US Department of Energy, Office of Science, Office of Basic Energy Sciences under Contract No. DE-AC02-76SF00515. The authors appreciate assistance from A. Mehta and D. van Campen (synchrotron XRD measurements), C. Xiang (Figure 2 graphics), and S. Mitrovic (XPS measurements).

1. B. A. Pinaud, J. D. Benck, L. C. Seitz, A. J. Forman, Z. Chen, T. G. Deutsch, B. D. James, K. N. Baum, G. N. Baum, S. Ardo, H. Wang, E. Miller and T. F. Jaramillo, *Energy Environ. Sci.*, 2013, **6**, 1983-2002.
2. (a) F. E. Osterloh and B. A. Parkinson, *MRS Bull.*, 2011, **36**, 17-22; (b) M. G. Walter, E. L. Warren, J. R. McKone, S. W. Boettcher, Q. Mi, E. A. Santori and N. S. Lewis, *Chem. Rev.*, 2010, **110**, 6446-6473; (c) H.-J. Lewerenz and L. Peter, *Photoelectrochemical Water Splitting*, The Royal Society of Chemistry, 2013; (d) S. Hu, C. Xiang, S. Haussener, A. D. Berger and N. S. Lewis, *Energy Environ. Sci.*, 2013, **6**, 2984.
3. S. Haussener, C. Xiang, J. M. Spurgeon, S. Ardo, N. S. Lewis and A. Z. Weber, *Energy Environ. Sci.*, 2012, **5**, 9922-9935.
4. J. Jin, K. Walczak, M. R. Singh, C. Karp, N. S. Lewis and C. Xiang, *Energ Environ Sci*, 2014, **7**, 3371-3380.
5. (a) F. E. Osterloh, *Chem. Mater.*, 2008, **20**, 35-54; (b) S. J. A. Moniz, S. A. Shevlin, D. J. Martin, Z.-X. Guo and J. Tang, *Energy Environ. Sci.*, 2015, **8**, 731-759.
6. Y. Park, K. J. McDonald and K.-S. Choi, *Chem. Soc. Rev.*, 2013, **42**, 2321-2337.
7. S. Hu, N. S. Lewis, J. W. Ager, J. Yang, J. R. McKone and N. C. Strandwitz, *J. Phys. Chem. C*, 2015, **119**, 24201-24228.
8. (a) K. Sun, F. H. Saadi, M. F. Lichterman, W. G. Hale, H.-P. Wang, X. Zhou, N. T. Plymale, S. T. Omelchenko, J.-H. He, K. M. Papadantonakis, B. S. Brunschwig and N. S. Lewis, *Proc. Natl. Acad. Sci. U. S. A.*, 2015, **112**, 3612-3617; (b) S. Hu, M. R. Shaner, J. A. Beardslee, M. Lichterman, B. S. Brunschwig and N. S. Lewis, *Science*, 2014, **344**, 1005-1009.
9. (a) J. A. Seabold and N. R. Neale, *Chem. Mater.*, 2015, **27**, 1005-1013; (b) L. Zhou, Q. Yan, A. Shinde, D. Guevarra, P. F. Newhouse, N. Becerra-Stasiewicz, S. M. Chatman, J. A. Haber, J. B. Neaton and J. M. Gregoire, *Adv. Energy Mater.*, 2015, **5**, 1500968.
10. A. Jain, S. P. Ong, G. Hautier, W. Chen, W. D. Richards, S. Dacek, S. Cholia, D. Gunter, D. Skinner, G. Ceder and K. A. Persson, *APL Mater.*, 2013, **1**, 011002.
11. K. A. Persson, B. Waldwick, P. Lazic and G. Ceder, *Phys. Rev. B*, 2012, **85**, 235438.
12. *Corrosion Mechanisms in Theory and Practice*, CRC Press, 3rd edn., 2011.
13. J. R. O'Dea, M. E. Holtz, A. E. Legard, S. D. Young, R. G. Burns, A. R. Van Wassen, D. A. Muller, H. D. Abruña, F. J. DiSalvo, R. B. van Dover and J. A. Marohn, *Chem. Mater.*, 2015, **27**, 4515-4524.
14. (a) M. Voith, G. Luckeneder and A. W. Hassel, *J. Solid State Electrochem.*, 2012, **16**, 3473-3478; (b) J.-P. Grote, A. R. Zeradjanin, S. Cherevko and K. J. J. Mayrhofer, *Rev. Sci. Instrum.*, 2014, **85**, 104101.
15. M. C. Biesinger, L. W. M. Lau, A. R. Gerson and R. S. C. Smart, *Appl. Surf. Sci.*, 2010, **257**, 887-898.
16. Y. Maimaiti, M. Nolan and S. D. Elliott, *Phys Chem Chem Phys*, 2014, **16**, 3036-3046.
17. G. Pacchioni, *ChemPhysChem*, 2003, **4**, 1041-1047.
18. Q. H. Wu, A. Thissen, W. Jaegermann and M. L. Liu, *Appl Surf Sci*, 2004, **236**, 473-478.